Research in Astron. Astrophys. **2013** Vol. **13** No. **7**, 862–874
http://www.raa-journal.org *http://www.iop.org/journals/raa*

***R**esearch in*
***A**stronomy and*
***A**strophysics*

Reflectance conversion methods for the VIS/NIR imaging spectrometer aboard the Chang'E-3 lunar rover: based on ground validation experiment data *

Bin Liu[1,3], Jian-Zhong Liu[1], Guang-Liang Zhang[1], Zong-Cheng Ling[2], Jiang Zhang[2], Zhi-Ping He[4], Ben-Yong Yang[5] and Yong-Liao Zou[1]

[1] National Astronomical Observatories, Chinese Academy of Sciences, Beijing 100012, China; *liub@nao.cas.cn*
[2] School of Space Science and Physics, Shandong University at Weihai, Weihai 264209, China
[3] Graduate University of Chinese Academy of Sciences, Bejing 100049, China
[4] Shanghai Institute of Technical Physics, Chinese Academy of Sciences, Shanghai 200083, China
[5] Anhui Institute of Optics and Fine Mechanics, Chinese Academy of Sciences, Hefei 230031, China

Received 2012 May 28; accepted 2013 February 4

Abstract The second phase of the Chang'E Program (also named Chang'E-3) has the goal to land and perform in-situ detection on the lunar surface. A VIS/NIR imaging spectrometer (VNIS) will be carried on the Chang'E-3 lunar rover to detect the distribution of lunar minerals and resources. VNIS is the first mission in history to perform in-situ spectral measurement on the surface of the Moon, the reflectance data of which are fundamental for interpretation of lunar composition, whose quality would greatly affect the accuracy of lunar element and mineral determination. Until now, in-situ detection by imaging spectrometers was only performed by rovers on Mars. We firstly review reflectance conversion methods for rovers on Mars (Viking landers, Pathfinder and Mars Exploration rovers, etc). Secondly, we discuss whether these conversion methods used on Mars can be applied to lunar in-situ detection. We also applied data from a laboratory bidirectional reflectance distribution function (BRDF) using simulated lunar soil to test the availability of this method. Finally, we modify reflectance conversion methods used on Mars by considering differences between environments on the Moon and Mars and apply the methods to experimental data obtained from the ground validation of VNIS. These results were obtained by comparing reflectance data from the VNIS measured in the laboratory with those from a standard spectrometer obtained at the same time and under the same observing conditions. The shape and amplitude of the spectrum fits well, and the spectral uncertainty parameters for most samples are within 8%, except for the ilmenite sample which has a low albedo. In conclusion, our reflectance conversion method is suitable for lunar in-situ detection.

Key words: instrumentation: detectors — lunar in-situ detection: VNIS — reflectance conversion: BRDF

* Supported by the National Natural Science Foundation of China.

1 INTRODUCTION

With the successful launch of the Chang'E-2 satellite on 2010 October 1, the second phase of the Chang'E (CE) program had begun. In 2013, CE-3 will land on the lunar surface and deliver a rover to perform in-situ detection. One of the important scientific goals of the CE-3 program is to develop in-situ detection for lunar mineral resources and composition. To reach this target, a VIS/NIR Imaging Spectrometer (VNIS) based on the Acousto-Optic Tunable Filter (AOTF) technique has been selected as one payload of the CE-3 lunar rover (He et al. 2011). AOTF based imaging and non-imaging spectrometers have been widely used in deep-space exploration (Trivedi et al. 2006), e.g. an Acousto-Optic Imaging Spectrometer (AIMS) was built as a candidate for Mars land rovers (Glenar et al. 2003). The main VNIS parameters are shown in Table 1. The spectral range for VNIS is from 0.45 μm to 2.4 μm. Lunar minerals can be effectively recognized in this spectral coverage. Lunar reflectance spectral data derived by VNIS represent the key to interpreting lunar composition, the conversion accuracy of which will greatly affect the accuracy of lunar element and mineral determination.

Table 1 Parameters of CE-3's VNIS Instrument

Spectral Range	450∼2400 nm
Spectral Resolution	$\leq$8 nm@450∼950 nm, $\leq$12 nm@900∼2400 nm
Bands	100@450∼950 nm, 300@900∼2400 nm
Corresponding RF Frequency	40∼180 MHz
Field of view	$\geq 6^\circ \times 6^\circ$(VIS), $\geq 3^\circ \times 3^\circ$(NIR)
Wavelength Selection	Continuously tunable
Image signal-to-noise ratio	$\geq$30

CE-3 would be the first program in history to carry an imaging spectrometer to the Moon for in-situ detection. For a long time, Earth based telescopes and spaceborne spectrometers have been the main methods for detection of lunar materials. Although the unmanned Luna missions and manned Apollo missions completed in-situ detection on the lunar surface, they did not carry imaging spectrometers (Ouyang 2005). Earth based telescopes and spaceborne spectrometers usually select the Apollo 16 landing site, the Cayley Plains, as a calibration target, and take the laboratory spectrum of lunar sample 62231 after using the spectrometer response as a standard to calibrate the reflectance of other areas (Pieters 1999; Pieters et al. 2009). The CE-3 rover will land on Sinus Iridum, the detection area of which will not include the Cayley Plains area. So, we cannot use reflectance conversion methods from telescopes on Earth or spaceborne spectrometers in VNIS data. This mode of detection needs new reflectance conversion methods.

In-situ detection by imaging spectrometers has been widely used (Guinness et al. 1987; Reid et al. 1999; Bell et al. 2003) for rovers on Mars (Viking lander, Pathfinder, Spirit and Opportunity), and we could learn from the experience of those missions. The Viking lander's multi-spectral camera calculated radiance factor (I/F), which is one kind of bidirectional reflectance (Hapke 1993). I/F data are also widely used by the Hubble Space Telescope and spaceborne imaging spectrometers (Bell et al. 1999; Bell 2008). The imager for Mars Pathfinder (IMP) calculated reflectance factor R* (or reflectance coefficient) for the first time (Reid et al. 1999). Spirit and Opportunity were launched in 2003 (Bell et al. 2003). The Pancam cameras aboard these two rovers calculated reflectance data of both I/F and R*; Pancam also considered the effect of Mars' dust and built a bidirectional reflectance distribution function (BRDF) model for the rover's calibration target (Bell et al. 2006).

The Martian environment is very different from that of the Moon. The operation of the CE-3 lunar rover will also be divergent from those of Mars rovers. Thus it is worth discussing whether the reflectance conversion methods used on Mars are suitable for lunar in-situ detection. Based on a survey of Mars employing reflectance conversion methods, we analyze simulated lunar soil BRDF

data from a laboratory to evaluate the suitability of this approach. Furthermore, we establish methods for performing the reflectance conversion of VNIS and validate its feasibility by results from ground based experiments.

2 REFLECTANCE CONVERSION METHODS USED ON MARS

There are two methods that have been used to derive reflectance from landing rovers on Mars. One is to approximate I/F using radiance data. The other way is to derive R* by observing the calibration target. Detailed procedures of each method are as follows.

2.1 Deriving I/F

I/F, which is also called the radiance factor (Hapke 1993), is the ratio of the radiance observed from a surface to that of a perfectly white Lambertian surface illuminated by the same light, but at normal incidence. I is the radiance data observed from the scene and πF is the incident solar irradiance from above the Martian surface. The method for deriving I/F for the multispectral camera aboard the Viking lander (Guinness et al. 1987) is

$$\rho_j = \frac{[V_j - V_{j,\mathrm{shadow}}]}{\exp[-\iota/\mu_0]K_j \int I_0(\lambda)S_j(\lambda)d\lambda}, \tag{1}$$

where j represents the jth channel, ρ_j is I/F, and V_j is the sensor's voltage received from the jth channel, which includes the contribution from all incident light. $V_{j,\mathrm{shadow}}$ refers to the voltage received from all the scattered light, ι is the atmospheric optical depth, $I_0(\lambda)$ is the solar spectral irradiance, μ_0 the cosine of the incidence angle relative to the zenith, K_j the preflight calibration constant of the jth channel, and $S_j(\lambda)$ is the spectral responsivity of the jth channel. This method removed the effect of atmospheric and scattered sky light, deriving an uncertainty of less than 10%. The method used for Pancam in deriving I/F (Bell et al. 2006) is as follows: use the radiance spectrum at the top of the Earth's atmosphere, which is scaled to values on Mars' surface as observed through each Pancam filter with incident radiance scale factors, divided by the Pancam radiance data. This method is only approximate, because it does not consider the effect of Mars' atmosphere.

2.2 Deriving Reflectance Factor (R*)

IMP (Reid et al. 1999) calculated R* in the following way

$$R_{\lambda,\mathrm{sample}}(i,e,g) = \frac{I_{\lambda,\mathrm{sample}}(i,e,g)}{I_{\lambda,\mathrm{std}}(i,e,g)} R_{\lambda,\mathrm{std}}(i,e,g)\,. \tag{2}$$

$I_{\lambda,\mathrm{sample}}(i,e,g)$ is the sample's radiance data at a fixed geometry for light incident angle i, emergence angle e and phase angle g. $I_{\lambda,\mathrm{std}}(i,e,g)$ is the calibration target's radiance at the same geometry, and $R_{\lambda,\mathrm{std}}(i,e,g)$ is the calibration target's reflectance coefficient.

It is straightforward to directly compare reflectance factor data with laboratory spectra and spectra taken at different times of a day (Bell et al. 2006). It also has the advantage of being partially "atmospherically corrected." This method needs a calibration target with the property of being nearly a Lambertian surface, but the calibration target of IMP is not a perfect Lambertian surface; it has a strong opposition surge and specular reflection (Reid et al. 1999). This phenomenon also exists in the Pancam calibration target (Bell et al. 2003). To remove this effect, Bell et al. (2003) developed a model based on the BRDF measurements of the laboratory Pancam calibration target. This model combined the backscattering equation (Hapke 1986) with the He-Torrence model (He et al. 1991) and returned R* data. A model has also been developed for the Pancam calibration target to eliminate the effect of dust with different thicknesses on reflectance conversion (Bell et al. 2006).

2.3 Relationship Among Different Reflectance Data

We have referenced two sets of reflectance data: I/F and R*. Recently, the Moon Mineralogy Mapper (M3) on Chandrayaan-1 derived a new type of reflectance data called apparent reflectance (Green et al. 2011). It is worth discussing the relationships among these types of reflectance data. Although apparent reflectance is not referenced in Hapke's theory, by comparing results (Bell et al. 2006; Green et al. 2011), we found that apparent reflectance and R* are the same expression. Radiance factor differs from the other two reflectances by the cosine of the solar incidence angle, which is a constant that does not change the shape of the spectra.

3 SUITABILITY ANALYSIS OF USING MARS REFLECTANCE METHODS FOR LUNAR IN-SITU DETECTION

I/F and R* calibrated images are both constrained by the following assumptions (Bell et al. 2006): (1) All illumination comes directly from a point source at the Sun. (2) The scene being imaged is perfectly flat. (3) The scene elements being imaged are Lambertian.

The lunar environment is quite different from Mars in terms of the atmosphere, temperature changes, surface composition etc. It is important to discuss whether Mars' reflectance conversion methods are suitable for lunar in-situ detection.

3.1 Suitability Analysis

We will analyze whether lunar in-situ detection by CE-3 satisfies the three assumptions as follows:

Firstly, the lunar environment has almost no atmosphere; the incident light to one point O on the lunar surface all comes from the Sun's surface. We could calculate the field angle $\Delta\theta$ from point O to the Sun's surface

$$\Delta\theta \approx \frac{D}{d} \approx 32' \,, \tag{3}$$

where D is the solar diameter (1.392×10^9 m), and d (1.496×10^{11} m) is the distance between point O and the Sun's surface. $\Delta\theta$ is so small that we can consider all lunar surface illumination as coming from a point source in the direction of the Sun.

Secondly, the CE-3 rover will land on a smooth surface in the region of Sinus Iridum, which is an impact basin filled with basalt, and it is half-surrounded by Montes Jura. VNIS will be set at the front of the land rover; it has a height of 0.65 meters, and the field of view is 6°. The detection angle of VNIS is fixed at 45°. We can calculate the area of the scene being imaged as $0.13\times0.13\,\mathrm{m}^2$, which is so small that we could consider it to be flat.

Finally, the scene being imaged should be Lambertian according to the assumption. It is a good assumption for the surface of Mars when we do not necessarily know the surface BRDF (Hapke 1986; Hapke 1981, 1984). As is well known, the lunar surface is not a Lambertian surface (Hapke 1986), but is a surface with specular reflection, multiple scattering, opposition effect, etc. To remove these effects, photometric normalization must be done after reflectance conversion (McEwen 1996). The goal of photometric normalization is to normalize reflectance data of different incident and emergence angles to the same viewing geometry.

During the process of photometric normalization, we should first select a suitable photometric function. Researchers have developed many photometric models to describe the lunar surface's photometric characteristics, i.e. the Lommel-Seelinger empirical model and Hapke model, based on the radiative transfer equation (Hillier et al. 1999). However, these models were mainly developed relying on data from telescopes and satellites. So, it is worth discussing whether could we consider the lunar surface to be Lambertian when the imaging area is small and so close. We can use simulated lunar soil's BRDF data to aid this discussion.

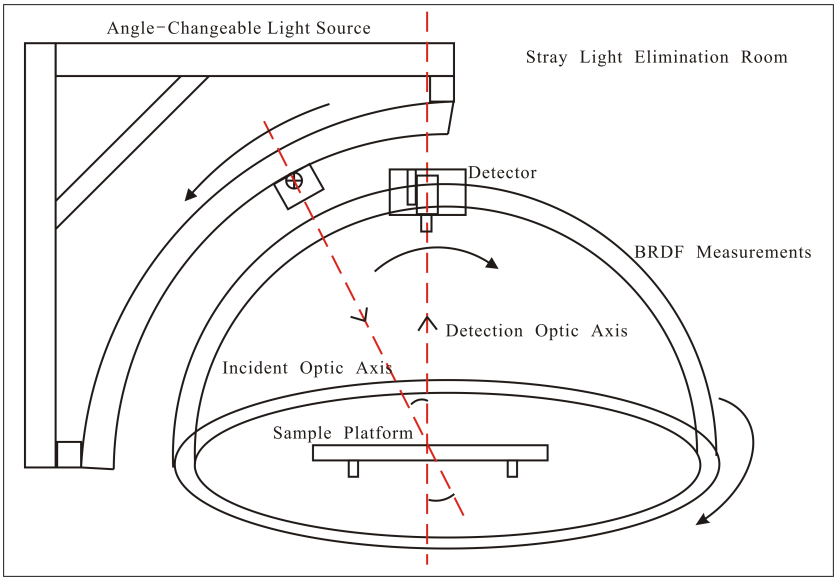

Fig. 1 BRDF device and measurement principle. Illumination incident angle could be changed by the movement of the light source; viewing detector's detection angle and azimuth angle could be changed by the movement of detector and the guide rail.

3.2 Data Analysis of BRDF for Simulated Lunar Soil

We simulated the detection model for VNIS in the laboratory and present the results of this lunar simulated soil (Chang'E program simulated lunar soil preparation report, 2007) as being representative of the natural conditions in real lunar soil. We can thus analyze its BRDF characteristics.

Figure 1 demonstrates the BRDF devices and method used for measurement. Yang et al. (2009) explains the methods of how to measure the sample's BRDF. Three kinds of simulated lunar soil were prepared by the National Observatories, Chinese Academy of Sciences: Lunar Low-Ca basaltic (LLB) soil, Lunar High-Ca basaltic (LHB) soil and Lunar highland plagioclase (LP) soil. The laboratory BRDF of the LLB was measured at Anhui Institute of Optics and Fine Mechanics, Chinese Academy of Sciences, because the CE-3 rover will land on Sinus Iridum, the composition of which is mostly low-Ca basaltic soil.

The LLB's BRDF (Fig. 2) was measured by changing the incident angle of the light, detector's angle and detector's azimuth angle (the angle between the detection plane, which includes the sensor and sample platform's normal, and the light plane, which includes the light source and sample platform's normal). Light incident angles were selected at 5°, 15° and 30°. Values for the azimuth angle were 25°, 55°, 85°, 115°, 145° and 175°, and values for the detection angle of the sensor were 10°, 20°, 30°, 40°, 50°, 60° and 70°. The calibration target was calibrated by the Anhui Institute of Optics and Fine Mechanics. The source of measurement errors is mainly error in the calibration target's 0°/45° reflectance coefficient conversion, and changes in the irradiance uniformity caused by lighting and detection geometry. The measurement uncertainty is between 2.4%–3.6%.

Figure 2(a) shows that the opposite effect exists in simulated lunar soil when the incidence angle is 5°, and emergence angle equals 0°, where the BRDF values are higher than those for other angles. From Figure 2(b) and (c) we can see when emergence angles are equal or close to the incident angles, the BRDF values become higher. This is especially obvious when the azimuth angle equals 175°.

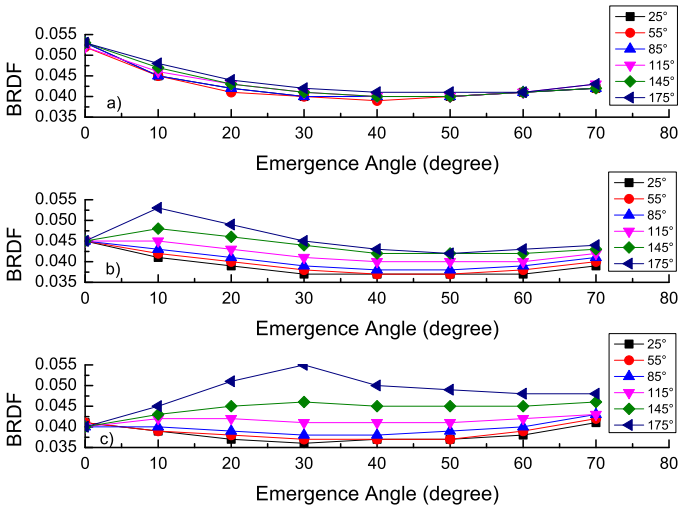

Fig. 2 Simulated Lunar Low-Ca Basaltic (LLB) soil BRDF data: a) Illumination incident angle equals 5°; b) Illumination incident angle equals 15°; c) Illumination incident angle equals 30°.

This phenomenon is caused by the specular reflection effect. These results demonstrate that the lunar surface can still not be considered to be a Lambertian surface when performing in-situ detection. So, the third assumption may be not suitable for the lunar surface. Actually, Mars' surface is also not Lambertian; specular and opposition effects exist based on data from the Viking landers, Pathfinder and the MER multi-spectral camera (Regner et al. 1988; Johnson et al. 1999; Johnson et al. 2006). From the BRDF data of IMP and Pancam, the calibration target cannot be considered as an ideal Lambertian surface either, which also has a "hotspot" caused by specular and opposition effects.

In conclusion, the first and second assumptions are reasonable for lunar in-situ detection, but the third assumption is not. As we have discussed, photometric normalization must be done after reflectance conversion to remove the effect of different viewing geometry. To do photometric normalization well, we should also implement a photometric data acquisition strategy like IMP and Pancam (Johnson et al. 1999; Johnson & Team 2004). For brevity we will not discuss photometric normalization in this paper.

4 REFLECTANCE CONVERSION METHOD AND VALIDATION OF VNIS

In this section, we transformed Mars reflectance conversion methods to be applicable for observations on the lunar surface based on the suitability analysis. To validate the effectiveness of our methods, data from the ground validation experiment of VNIS are used.

4.1 Ground Validation Experiment for VNIS

Before the CE-3 imaging spectrometer (VNIS) is brought to the lunar surface, many ground validation experiments should be performed. There are two main objectives for ground validation experiments; one is to evaluate the quality of its image and spectrum, and the other is to exercise its data processing methods. Reflectance data from the VNIS were validated by comparison with a standard spectrometer (ASD). The ASD instrument we used here is Field Spec 3, the performance and specification of which can be referenced from the website (*http://www.asdi.com*). The instrument's operation and geometry are different from those of the Mars multi-spectral cameras. There is a dust

cover aboard VNIS that prevents lunar dust from falling on the calibration target; this dust cover will be opened when the spectrometer is operating and it will be closed when the spectrometer is not operating. To avoid a high working temperature for the rover, the geometry of VNIS will be restricted to a solar elevation angle from 15° to 33°. Thus the light incident angle will change from 57° to 75°. The emergence angle will be fixed at 45°.

During the process of ground validation experiments, ASD and VNIS were fixed on the rover, which simulated the detection conditions on the lunar surface.

Figure 3 shows devices used in the validation experiment and the measurement process. The light sources usually used in the laboratory are xenon and halogen lamps; irradiance among sunlight, xenon and halogen lamps are compared in Figure 4. The incident angles of light sources were set from 45° to 80°, with a sampling interval of 5° The detection angles were fixed at 45°, and the azimuth angle changed from 30° to 180°, with a sampling interval of 30°. These two spectrometers firstly measured the calibration target's spectrum at the same time and with the same viewing geometry. After the calibration target was detected, we changed the target to the experiment samples. The raw data calibration process for VNIS and ASD included dark current subtraction and radiance calibration.

Figure 5 shows the pipeline for reflectance conversion and validation for the VNIS.

To simulate the lunar surface's composition and particle sizes, five kinds of earth minerals were selected as experimental samples; they are hyperthene, diopside, olivine, feldspar and ilmenite. These minerals are characterized by obvious spectral features, which can be easily identified by VNIS and ASD. The mineral samples were ground with a grinder before the experiment, and the median particle size of the samples was controlled to be 40–130 μm. Major element microprobe analysis of hyperthene, diopside, olivine and feldspar is given in Table 2. In addition, 99% of ilmenite was composed of TiO_2. We also made seven mixture samples to simulate lunar soil by mixing and stirring four minerals of hyperthene, olivine, feldspar and ilmenite in the proportions shown in Table 3. The aim of the mixture samples was to utilize some minerals reduction models by linking mineral composition to reflectance absorption features.

4.2 Conversion and Validation of I/F for VNIS

Firstly, we calculate the solar irradiance at the lunar surface through every AOTF imaging spectrometer's band pass, and then set up a look-up table. Dividing the instrument's radiance data, which have been calibrated by results in the look-up table, we get I/F data in a fast and simple way

$$R_j = \frac{\pi I_j}{\int I_0(\lambda) S(\lambda) d\lambda}, \tag{4}$$

where R_j is I/F in the jth band, I_j is the radiance data for the jth band image, $I_0(\lambda)$ is the solar irradiance on the lunar surface, and $S(\lambda)$ is spectral responsivity for the imaging spectrometer of an image in the jth band.

Figure 6 demonstrates a comparison of the results between samples of the I/F spectrum taken with ASD and VNIS. We found that the shape and value of reflectance data from the VNIS are similar and close to those from standard ASD reflectance data, but we note that at some wavelengths, the VNIS reflectance spectrum is not as smooth as the one from ASD, especially in the spectral range 450–950 nm. There are two probable reasons for this. One is that the intensity of the laboratory light sources is too weak; although the intensity of xenon is much stronger than the halogen lamp in the spectral range 450–950 nm, it is still weak and unstable compared to light from the Sun. The integration time for bands taken with VNIS was set for the intensity of sunlight. When the light source changed from sunlight to xenon, the signal detected by VNIS was weak, which decreased the signal to noise ratio (SNR) of VNIS. The other reason is that standard reflectance data from the ASD are averaged from ten repeated measurements, but reflectance data from VNIS are not averaged. We

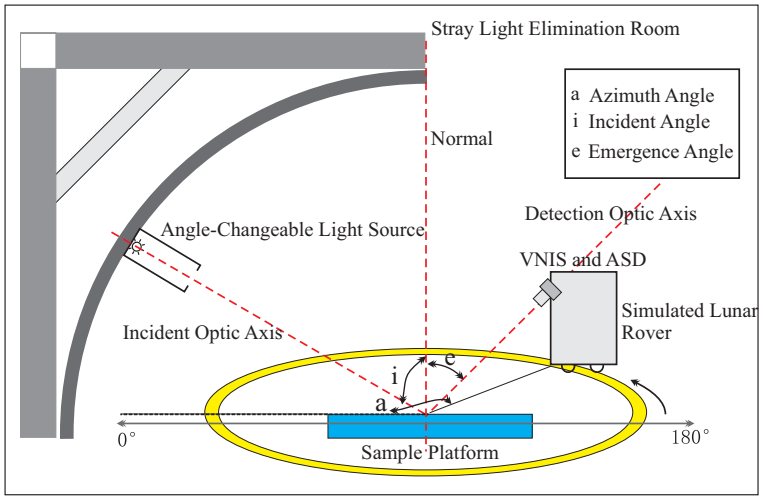

Fig. 3 VNIS ground science validation experiment devices and measurement principle. The validation experiment simulates the conditions of the CE-3 lunar rover's work mode on the lunar surface.

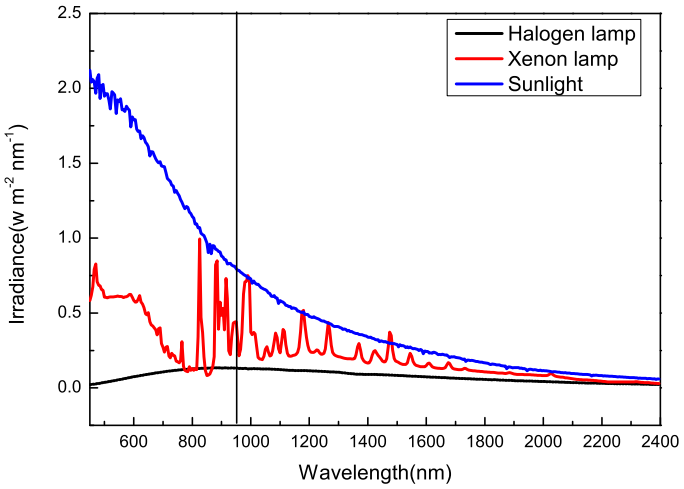

Fig. 4 Iradiance comparison between sunlight and laboratory experiment light sources, during the ground validation experiment for VNIS in the laboratory. A xenon light source was used in VIS-NIR bands (450–950 nm) and a halogen light source was selected in infrared bands (900–2400 nm).

also noted jitter in the spectrum from ASD near 1000 nm and 2000–2400 nm. This phenomenon exists in most ASD spectrometers. There is a junction between the two ASD detectors at the spectral position of 1000 nm, which caused the jitter at this position, but the jitter in the range 2000–2400 nm is mainly caused by the detector's low spectral response.

Spectral uncertainty is an assessment parameter which could tell us quantitatively the deviation of VNIS reflectance from ASD data. We calculate spectral uncertainty parameters between VNIS

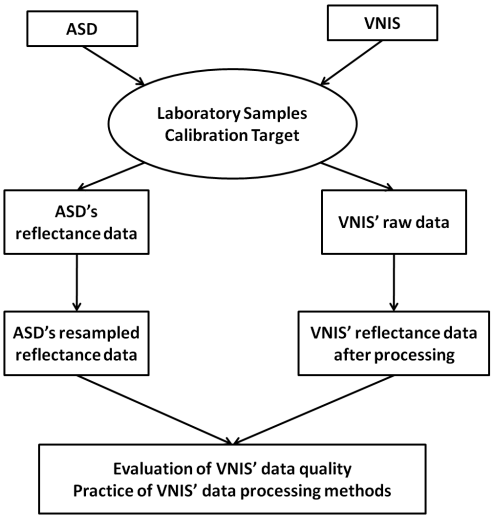

Fig. 5 Reflectance conversion and validation pipeline for VNIS.

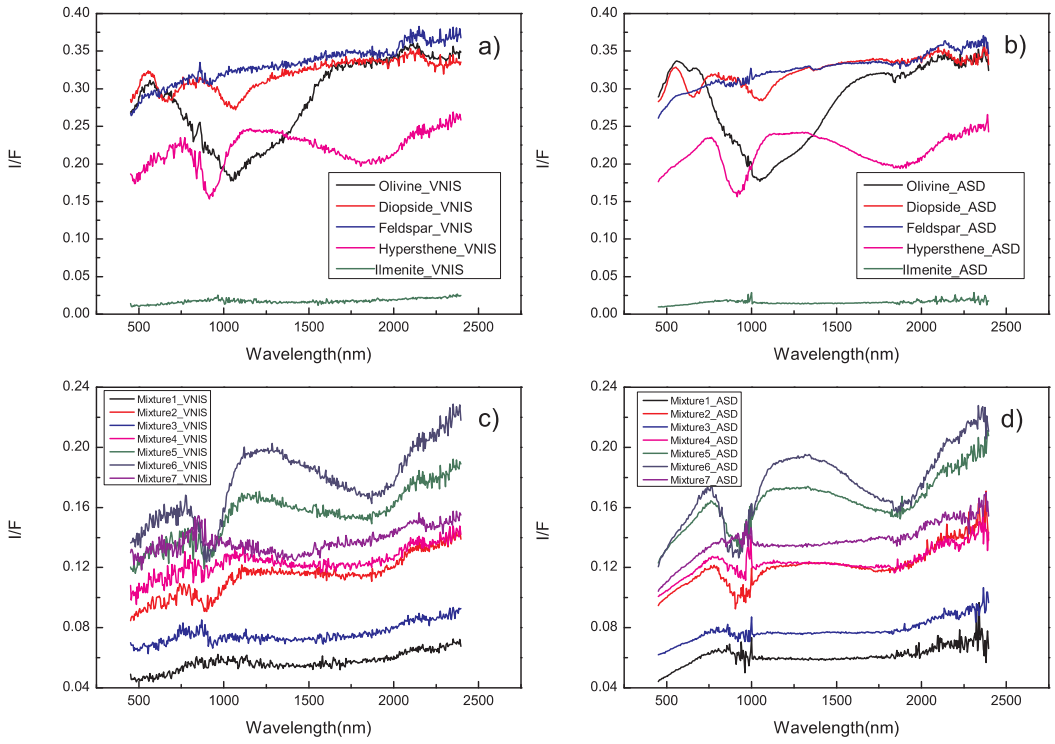

Fig. 6 Experiment sample's radiance factor (I/F) spectrum comparison between VNIS and ASD; the geometry is as follows: incident angle $i = 60°$, emergence angle $e = 45°$, azimuth angle $a = 180°$. a) VNIS' I/F of five minerals, b) ASD's I/F of five minerals. c) VNIS' I/F of seven mixtures, d) ASD's I/F of seven mixtures.

Table 2 Element Analyses of Hyperthene, Diopside, Olivine and Feldspar

Oxide	Hyperthene	Diopside	Olivine	Feldspar
SiO_2	53.64	55.72	41.89	56.14
TiO_2	0.12	0.08	0.02	0.03
Al_2O_3	3.72	0.16	0.02	27.62
Cr_2O_3	0.23	0.53	0.01	0.01
FeO	17.31	1.24	8.62	0.08
NiO	0.04	0.02	0.38	0.01
MnO	0.29	0.06	0.13	0.01
MgO	24.73	17.23	49.18	0.02
CaO	0.49	24.45	0.06	10.44
Na_2O	0.02	0.37	0.02	5.13
K_2O	0.01	0.01	0.01	0.37
Total	100.60	99.87	100.31	99.87

Table 3 Proportion of Seven Mixtures

Sample Name	Hyperthene (wt%)	Olivine (wt%)	Feldspar (wt%)	Ilmenite (wt%)
Mixture1	10	20	30	40
Mixture2	40	30	20	10
Mixture3	20	40	10	30
Mixture4	30	10	40	20
Mixture5	45	0	50	5
Mixture6	60	5	35	0
Mixture7	0	15	70	15

and ASD reflectance data, and the calculation function is shown in Equation (5)

$$\delta s = \frac{\sum_{i=1}^{N} \left| \frac{S_{\mathrm{VNIS},i} - S_{\mathrm{ASD},i}}{S_{\mathrm{ASD},i}} \right|}{N} \times 100\%, \tag{5}$$

where δs is the spectral uncertainty parameter, $S_{\mathrm{VNIS},i}$ is the ith band reflectance data of VNIS, and $S_{\mathrm{ASD},i}$ is the ith band reflectance data of ASD. Table 4 demonstrates all the samples' spectral uncertainty results. The spectral uncertainty of most samples is less than 8%, except for ilmenite. Because the color of ilmenite is black, its albedo is very low, which makes the signal weak, and brings down the SNR of VNIS, so the spectral uncertainty of ilmenite is higher than other samples.

4.3 R* Conversion

The reflectance factor could be calculated because there is a calibration target on VNIS. Like Pancam, when VNIS worked in calibration mode, the detection object changed from the lunar surface to the calibration target. The reflectance products of the multispectral cameras aboard Clementine, CE-1 and Chandrayaan-1 are also the reflectance factor (Pieters 1999; Pieters et al. 2009), so it is convenient to compare these reflectance data.

VNIS's work mode and geometry are different from the Mars multispectral cameras, with considerations for the dust cover and solar elevation angle as noted earlier. Hence, a different BRDF model should be set up to act as a calibration target.

The proposed procedures for conversion of the spectrometer's reflectance factor are as follows:

(1) Measure and calculate reflectance factor data $R_{\lambda,\mathrm{lab}}(i, e, g)$ for the calibration target using the working geometries of VNIS in ground laboratory experiments with the methods of Yang et al. (2009);

Table 4 Spectral Uncertainty In I/F From the Laboratory Results

Samples	450∼950 nm (δ_s)	900∼2400 nm (δ_s)
Hyperthene	4.23	2.17
Diopside	1.62	2.10
Olivine	5.44	2.86
Feldspar	2.98	2.36
Ilmenite	12.99	14.13
Mixture1	5.51	6.88
Mixture2	3.37	4.52
Mixture3	3.82	4.53
Mixture4	5.28	2.26
Mixture5	7.87	4.50
Mixture6	5.67	2.31
Mixture7	6.04	3.21

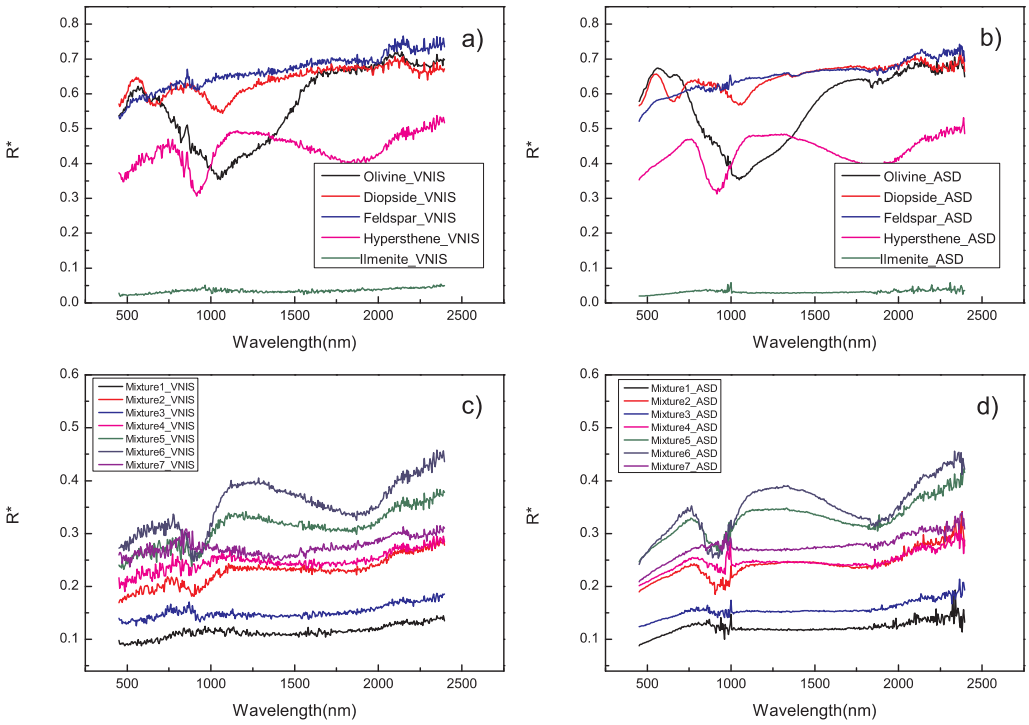

Fig. 7 A comparison of the spectrum for the experimental sample's reflectance factor between VNIS and ASD; the geometry is as follows: incident angle $i = 60^\circ$, emergence angle $e = 45^\circ$, azimuth angle $a = 180^\circ$. a) VNIS value of R* for five minerals, b) ASD value of R* for five minerals, c) VNIS value of R* for seven mixtures, d) ASD value of R* for seven mixtures.

(2) Resample the calibration target's laboratory spectrum $R_{\lambda,\mathrm{lab}}(i,e,g)$ into every band of a standard spectrum $R_{\lambda,\mathrm{std}}(i,e,g)$ for the instrument;
(3) Calculate R* ($R_{\lambda,\mathrm{sample}}(i,e,g)$) for the imaging area by Equation (2), which needs radiance data and $R_{\lambda,\mathrm{std}}(i,e,g)$.

Table 5 Laboratory Samples' R* Spectral Uncertainty Results

Samples	450∼950 nm (δ_s)	900∼2400 nm (δ_s)
Hyperthene	4.23	4.62
Diopside	3.64	1.65
Olivine	3.42	5.81
Feldspar	1.07	4.51
Ilmenite	10.67	14.50
Mixture1	3.84	5.21
Mixture2	3.21	2.63
Mixture3	4.41	2.22
Mixture4	5.28	5.27
Mixture5	4.79	1.44
Mixture6	4.79	4.19
Mixture7	3.97	2.40

Figure 7 shows a comparison of the results for the reflectance factor of the samples between ASD and VNIS. The shape and values of spectra taken by VNIS are similar and close to those taken by ASD in most wavelengths. Spectral jitter also exists in some bands, the reasons for which are the same as in I/F.

Table 5 demonstrates the spectral uncertainty parameters calculated from VNIS and ASD's R* spectrum; most samples' spectral uncertainty parameters are within 6%, but ilmenite is an exception due to its low albedo values.

5 CONCLUSIONS

Based on the experience gained from reflectance conversion methods developed for in-situ detection on Mars, we firstly analyze the suitability of the methods for lunar in-situ detection. According to data of simulated lunar soil taken by BRDF in a laboratory, it is not suitable to assume lunar detection is Lambertian because of opposition and specular effects, but we could apply photometric normalization to remove these effects by observing photometric data after reflectance conversion. By considering differences between the surfaces of the Moon and Mars, we improved and set up reflectance conversion methods for the CE-3 imaging spectrometer. Through ground experimental data describing the imaging spectrometer on CE-3, we validated the effectiveness of the methods. The shape and values of reflectance data from VNIS are similar and close to those of ASD's; the spectral uncertainty parameters of most samples are within 8%, excepted for ilmenite, because of its low albedo, which makes the signal received by VNIS and ASD too weak. The validation shows that our reflectance conversion methods are suitable and can be used in the CE-3 VIS/NIR imaging spectrometer. During the following ground and in-flight calibration experiments, we will continue to improve and validate our methods to produce better reflectance data.

Acknowledgements This study was supported by the Chang'E Program of China (No. TY3Q20110029), the Knowledge Innovation Program of the Chinese Academy of Sciences (Grant No. KGCX2-EW-402) and the National Natural Science Foundation of China (Grant Nos. 11003012 and U1231103).

References

Bell, J. F., Wolff, M. J., Daley, T. C., et al. 1999, Icarus, 138, 25

Bell, J. F., Joseph, J. N., Sohl-Dickstein, H. M., et al., 2006, J. Geophysics., Res., 111, E02S03

Bell, J. F., Squyres, S. W., Herkenhoff, K. E., et al. 2003, Journal of Geophysical Research (Planets), 108, 8063

Bell, J. 2008, The Martian Surface (New York: Cambridge Univ. Press), 154
Glenar, D. A., Blaney, D. L., & Hillman, J. J. 2003, Acta Astronautica, 52, 389
Green, R. O., Pieters, C., Mouroulis, P., et al. 2011, Journal of Geophysical Research (Planets), 116, E00G19
Guinness, E. A., Arvidson, R. E., Dale-Bannister, M. A., Singer, R. B., & Bruckenthal, E. A. 1987, J. Geophys. Res., 92, 575
Hapke, B. 1986, Icarus, 67, 264
Hapke, B. 1981, J. Geophysics. Res., 86, 3039
Hapke, B. 1993, Theory of Reflectance and Emittance Spectroscopy (New York: Cambridge Univ. Press), 262
He, X. D., Torrance, K. E., Sillion, F. X., & Greenberg, D. P. 1991, ACM SIGGRAPH Computer Graphics, 25, 175
He, Z., Shu, R., & Wang, J. Y. 2011, in Proceedings of SPIE, the International Society for Optical Engineering (Society of Photo-Optical Instrumentation Engineers)
Hillier, J. K., Buratti, B. J., & Hill, K. 1999, Icarus, 141, 205
Johnson, J. R., Bridges, N. T., Anderson, R., et al. 1999, J. Geophys. Res., 104, 8809
Johnson, J. R., & Team, A. S. 2004, AGU Fall Meeting Abstracts, A196
Johnson, J. R., Grundy, W. M., Lemmon, M. T., et al. 2006, Journal of Geophysical Research (Planets), 111, E02S14
McEwen, A. S. 1996, in Lunar and Planetary Institute Science Conference Abstracts, 27, 841
Ouyang, Z. Y. 2005, Introduction to Lunar Science, (Beijing: Chinese Astronautic Publishing House), 251
Pieters, C. M. 1999, in Workshop on New Views of the Moon II: Understanding the Moon Through the Integration of Diverse Datasets, 8025
Pieters, C. M., Boardman, J., Buratti, B., et al. 2009, Curr. Sci, 96, 500
Regner, P., Kamp, L., & Neukum, G. 1988, in Lunar and Planetary Institute Science Conference Abstracts, 19, 968
Reid, R. J., Rueffer, P., Gliem, F., et al. 1999, J. Geophys. Res., 104, 8907
Trivedi, S., Rosemeier, J., Jin, F., et al. 2006, in Society of Photo-Optical Instrumentation Engineers (SPIE) Conference Series, 6100, eds. H. J. Hoffman & R. K. Shori, 505
Yang, B. Y., Zhang, L. M., Shen, Z. G., et al. 2009, Optics and Precision Engineering, 17, 8 (in Chinese)